

State resolved translational energy distributions of Cl and HCl in the ultraviolet photodissociation of chloroethylenes

Yibo Huang, Yung-An Yang,^{a)} Guoxin He, Satoshi Hashimoto,^{b)} and Robert J. Gordon
Department of Chemistry (m/c 111), University of Illinois at Chicago, Chicago, Illinois 60607-7061

(Received 17 March 1995; accepted 27 June 1995)

Velocity-aligned Doppler spectroscopy was used to measure the speed distribution functions of HCl($v''=0-2, J''$) produced in the 193 nm photodissociation of vinyl chloride. A mechanism which is consistent with our present data as well with our earlier work is three center elimination of HCl followed by concerted but nonsynchronous isomerization of the vinylidene fragment, with some of the isomerization energy converted to kinetic energy of the recoiling fragments. In order to explain the vibrational dependence of the translational and rotational energy distributions, the mechanism is assumed to be vibrationally adiabatic. In addition, magic angle Doppler spectroscopy was used to measure the speed distribution functions of Cl atoms produced in the photodissociation of vinyl chloride and the three dichloroethylene isomers. Bimodal energy distributions were observed for both spin-orbit states, with the Cl($^2P_{1/2}$) fragment having more kinetic energy than Cl($^2P_{3/2}$). The data are consistent with competitive reaction on two potential energy surfaces. Adiabatic correlation, with some scrambling in the asymptotic region, provide a qualitative explanation of the spin-orbit branching ratios. © 1995 American Institute of Physics.

I. INTRODUCTION

A fundamental question in chemistry is how a molecule behaves when multiple reaction pathways are available. The photodissociation reactions of chloroethylene molecules are an ideal case for studying this problem. While simple enough for accurate structural and dynamical calculations, these bichromophoric molecules have multiple transition states on several potential energy surfaces and display a complex photochemistry.¹ This paper is part of an ongoing study in which the yields and state distributions of the fragments are used to deduce the microscopic reaction mechanism.

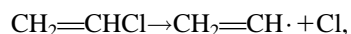
Considerable progress has been made in recent years in relating product state distributions of photo-initiated reactions to detailed features of the potential energy surface (PES).² If a molecule reacts directly on the initially excited PES, the rotational and vibrational populations of the fragments are related to the shape of the Franck-Condon region of the surface (e.g., via the rotational and vibrational reflection principles of Refs. 2 and 3). If instead of reacting directly the molecule is trapped in a long-lived resonance state of the same PES, the product state distribution reflects the properties of the transition state.⁴ But if the molecule first undergoes a radiationless transition, the product distribution provides information about the PES on which the reaction finally occurs. For example, a barrier in the exit channel can impart internal and translational energy to the fragments.⁵ Only when there is no exit barrier and the transition state is close to the product geometry is a statistical state distribution expected.⁶ While these general considerations were originally developed for molecules having a single reaction chan-

nel, they should apply just as well to more complex systems having multiple reaction paths.

To date there have been relatively few dynamical studies of molecules having multiple transition states. One molecule which has been studied in detail is ethylene.⁷ Excitation of the double bond is followed by internal conversion to the ground state, where H and H₂ products are formed. Very different mechanisms are involved for the two fragments. Hydrogen atoms are produced by a simple bond fission, while H₂ can be formed by three-center elimination, four-center elimination, and H atom migration followed by molecular elimination. Because of a large exit channel barrier, the peak translational energy of the H₂ fragment is much greater than zero.

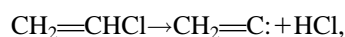
Replacing one or more hydrogen atoms with halogens considerably increases the complexity of the system.⁸ All of the chloroethylenes have a strong UV absorption band around 190 nm, which is assigned to transitions from $\pi(\text{CC})$ to $\pi^*(\text{CC})$, $\sigma^*(\text{CCl})$, and $4s$ Rydberg orbitals, as well as to an $n \rightarrow \sigma^*$ transition on the Cl atoms. Upon excitation, these molecules may undergo *cis-trans* isomerization, atomic detachment, molecular elimination, and H or Cl migration. These reactions may occur on the initially excited PES, on a different excited PES following an adiabatic transition, or on the ground PES following internal conversion.

The focus of this paper is mainly on vinyl chloride (VCl). The primary photochemistry of VCl has been studied extensively for several decades. The earliest work⁹ established that the major channels are C-Cl bond rupture,



$$\Delta H_{298}^0 = 89 \pm 2 \text{ kcal/mol} \quad (1)$$

and HCl elimination. The latter may proceed by either α , α elimination to produce vinylidene,

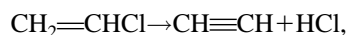


^{a)}Permanent address: DOTY Scientific, Inc., 700 Clemson Rd., Columbia, South Carolina 29223.

^{b)}Permanent address: Institute for Electronic Science, Hokkaido University, Sapporo 060, Japan.

$$\Delta H_{298}^0 = 67 \pm 2 \text{ kcal/mol} \quad (2)$$

or by α,β elimination to produce acetylene,



$$\Delta H_{298}^0 = 23.7 \pm 0.4 \text{ kcal/mol.} \quad (3)$$

These experiments were performed in the gas phase at relatively high pressure, using flash photolysis or photosensitized photolysis. Later bulk experiments employed a variety of techniques including excitation in a chemical laser¹ and in a cryogenic matrix,¹⁰ and IR multiphoton dissociation.¹¹ Recent studies were performed under collisionless (or low collision) conditions, using IR emission,¹² time-resolved FTIR,¹³ time-of-flight mass spectroscopy,¹⁴ and multiphoton ionization^{15,16,17} detection. Despite all of these previous studies, the reaction mechanism is still uncertain, owing to the multiple pathways available for each product.

It is generally agreed that photoelimination of HCl occurs on the ground (S_0) PES. The early chemical laser study by Berry¹ indicated that the primary mechanism for producing HCl is four-center α,β elimination. He observed a non-statistical vibrational distribution which he attributed to an impulsive mechanism. Berry introduced the idea of a localized available energy, which he defined as the difference between the potential energy at the crest of the elimination barrier and that of the separated products. In Berry's mechanism, the localized energy is partitioned between internal energy of HCl and relative translational energy of the fragments. Later, Umemoto *et al.*¹⁴ measured the translational energy distribution $p(E_t)$ of HCl at 193 nm. They found that $p(E_t)$ has a most probable value for $E_t > 0$. They concluded that HCl elimination is nonstatistical, and that only part of the energy is available to the HCl fragment, in agreement with Berry.

Different conclusions were reached in other experiments. Using IR multiphoton dissociation (also on the ground PES), Reiser *et al.*¹¹ revealed a preference for α,α elimination of HCl, and explained their data with a statistical, RRKM model. Using high resolution FTIR spectroscopy, Donaldson and Leone¹³ concluded that all of the available energy is partitioned statistically into the product modes of the transition state. Since HCl in the transition complex has a lower vibrational frequency than nascent HCl, the state distribution appears to be nonstatistical in the asymptotic region.

The velocity of the Cl fragment has been measured by time-of-flight mass spectrometry,¹⁴ by Doppler spectroscopy,^{18,19} and by photofragment imaging.²⁰ These studies revealed an asymmetric, bimodal velocity distribution function, which is indicative of simultaneous reaction on two PES's. Most likely there is competition between reactions on the n,σ^* and the ground PES. A nonstatistical population of spin-orbit states $\text{Cl}(^2P_j)$ was also observed. In contrast, H atoms have an isotropic, Maxwellian velocity distribution, which is indicative of a statistical reaction on the ground PES.

Recently, Morokuma and co-workers performed extensive calculations of the ground PES for all reaction channels of VCl and dichloroethylene (DCE).^{21,22} They systematically examined all three-center, four-center, and migration mecha-

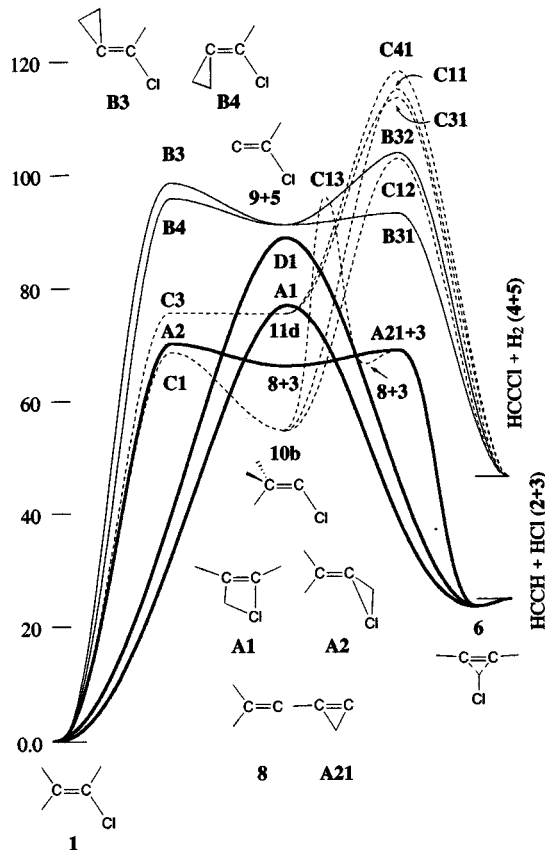


FIG. 1. Reaction paths on the ground PES of vinyl chloride, taken from Fig. 4 of Ref. 21. The potential energies (in kcal/mol) were calculated at the MP2/6-31G(d,p) level, using optimized geometries for HCl and H₂ elimination. Bold lines are for processes initiated by HCl elimination, solid lines are for those initiated by H₂ elimination, and dotted lines for those initiated by H or Cl migration. The numbers denote the following species: (1) VCl, (2) HCCH, (3) HCl, (4) HCCCl, (5) H₂, (6) HCCH-HCl π -complex, (8) vinylidene, :CCH₂ (9) chlorovinylidene, :CCHCl, (10) CH₂CCl, and (11) CH₂CICH. Letters refer to transition states calculated in Ref. 21.

nisms for molecular elimination. For VCl they calculated that the barriers for α,α and α,β elimination of HCl are 69.1 kcal/mol and 77.4 kcal/mol, respectively, as shown in Fig. 1 (peaks A2 and A1, respectively). They also discovered a "knockout" mechanism in which H migration precedes four-center elimination of HCl, with a barrier of 87.7 kcal/mol (D1 in Fig. 1). Except for α,α elimination, the dissociation pathways have substantial exit barriers. Their study predicts that α,α elimination is the dominant channel for HCl production.

Studies in our laboratory¹⁶ were performed using 193 nm to excite VCl and the three DCE isomers in a pulsed molecular beam, and resonance-enhanced multiphoton ionization (2+1 REMPI) to measure the state distributions of the fragments. For the HCl channel we found that the rotational state distribution for the ground vibrational state, $v''=0$, is qualitatively different from those for $v''=1$ and 2. For VCl, for example, we found that HCl($v''=0$) has a biexponential state distribution, with a low J component having a rotational "temperature" T_{rot} near 300 K (not caused by collisional relaxation) and a high J component having $T_{\text{rot}} \approx 20\,000$ K. In contrast, the rotational state distributions

for $v'' > 0$ are Boltzmann-type, with $T_{\text{rot}} \approx 2,000$ K. Neither distribution is statistical.

A plausible explanation of this dichotomy is that $\text{HCl}(v''=0)$ is produced by three-center, α, α elimination, while $v'' > 0$ is produced by four-center, α, β elimination. To test this hypothesis we measured the state distributions for α -deuterated VCl (CH_2CDCl , $d\text{-VCl}$).¹⁷ We discovered that the HCl yield from $d\text{-VCl}$ is only 25% of that from normal VCl , showing that the mechanism is primarily α, α elimination. This is in contrast to the behavior in solution, where HCl elimination occurs exclusively across the double bond. Surprisingly, we found that the rotational state distributions for HCl produced from the deuterated and normal compounds are indistinguishable, showing that some scrambling of rotational population must occur, either before or after the transition state is reached. In another experiment we found that the HCl rotational state distributions for all three isomers of DCE are qualitatively similar to those of VCl .²³ Both experiments show that the different behavior for $v''=0$ and $v'' > 0$ is *not* due simply to a branching between α, α and α, β elimination.

The nature of the scrambling process is still an open question. One possibility is that H migrates back and forth between the two carbon atoms before HCl is eliminated. If we assume that elimination occurs through a single (e.g., α, α) transition state, the HCl state distributions originating from VCl and $d\text{-VCl}$ will be identical, with the relative quantum yields determined by the rate of H migration. This mechanism is consistent with the finding of Riehl and Morokuma (RM) (Ref. 21) that the barrier for $\alpha\text{-H}$ migration is lower than that of any of the HCl elimination paths (see Fig. 1).

A second possibility is that a H atom shift (forming CHCH_2Cl) and HCl elimination are concerted, producing acetylene as the nascent product. The probabilities of forming a HCl bond between Cl and $\alpha\text{-H}$ or $\beta\text{-H}$ determine the relative quantum yields.

Still a third possibility is that scrambling of the rotational population occurs in the exit channel after HCl has been eliminated. Subpicosecond isomerization of vinylidene to form acetylene²⁴ while the fragments separate may erase the memory of the initial transition state to give identical rotational state distributions for α, α and α, β elimination. A variant of this mechanism is the formation of a short-lived σ or π complex¹¹ in the exit channel.

In an attempt to identify the microscopic mechanism, we used the method of velocity-aligned Doppler spectroscopy (VADS) (Ref. 25) to measure the speed distribution function of individual rovibrational states of HCl . Since the exit barrier for three-center elimination is very small (2.5 kcal/mol) compared with that for the four-center channel (52.5 kcal/mol),²¹ substantially different kinetic energy distributions should result from these two mechanisms. In principle, the three-center process is more likely to produce a statistical distribution, while the large barrier in the four-center mechanism should channel an excess of energy into translation and rotation. A concerted elimination mechanism could produce a hybrid of the two limiting cases. State-specific speed distribution functions, coupled with our knowledge of the rota-

tional populations and relative quantum yields, should help characterize the nature of the transition states.

State-resolved speed distribution functions can also be used to clarify the mechanism of Cl elimination. We have used the technique of magic angle Doppler spectroscopy (MADS) (Refs. 19 and 26) to determine the speed distributions of $\text{Cl}(^2P_{3/2})$ and $\text{Cl}(^2P_{1/2})$ produced from VCl and the three DCE isomers.

II. EXPERIMENTAL METHOD

The pump-and-probe apparatus used in this experiment has been described previously.¹⁶ All of the experiments were performed in a pulsed molecular beam machine equipped with a time-of-flight mass spectrometer (TOF-MS). A 193 nm ArF excimer laser (Lambda Physik EMG150, 10 mJ/pulse, 10 Hz) was used as the photolysis source. The beam diameter was reduced to ~ 2 mm by passing it through an iris and a 500 mm lens. An excimer-pumped, frequency-doubled dye laser (Lambda Physik LPX200/FL3002, ~ 1 mJ/pulse) was used to probe the nascent products by 2+1 REMPI. The probe beam was focused with a 150 mm lens to a spot size of ~ 0.1 mm. HCl was detected using the $F^1\Delta$ state as the resonant intermediate level.²⁷ $\text{Cl}(^2P_{3/2})$ and $\text{Cl}(^2P_{1/2})$ were detected at 474.464 and 475.616 nm, respectively.²⁸ An intracavity étalon narrowed the bandwidth of the fundamental to 0.04 cm^{-1} . Pressure tuning of the étalon was used in the VADS measurements and angle tuning in the MADS studies.

The photolysis laser was linearly polarized by a stack of ten quartz plates, which could be rotated to select the polarization direction. In conventional and velocity-aligned Doppler measurements, the pump and probe lasers were counter-propagated perpendicular to the direction of the gas expansion. In the MADS experiments, the lasers were aligned at a 135° angle, with the probe laser perpendicular to the molecular beam.

VCl was obtained from Fluka with a specified purity $>99.5\%$. Before use, the sample gas was subjected to a freeze-pump-thaw cycle. The dichloroethylenes were obtained from Aldrich with specified purities of 99% for *trans*- DCE , 97% for *cis*- DCE , and 98% for 1,1- DCE . They were stored in reservoirs and used without further purification. All sample gases were introduced into the vacuum chamber with a pulsed valve (Newport BV-100) at a stagnation pressure of ~ 200 Torr.

III. DOPPLER PROFILE ANALYSIS

The use of MADS and VADS to extract the speed distribution function has been described in a preliminary report. We review here only the essential results.

A. MADS

The Doppler shift of a particle having a velocity \mathbf{v} and a speed \mathbf{w} along the line-of-sight is given by

$$\nu = \nu_0(1 - \mathbf{w}/c), \quad (4)$$

where ν_0 is the frequency at the center of the line and c is the speed of light. If the particle has a speed distribution $f(v)v^2$ and anisotropy parameter β , its conventional Doppler spectrum is given by²⁹

$$D(w) = \int_{|w|}^{\infty} \frac{1}{2v} [1 + \beta P_2(\cos \theta_p) P_2(w/v)] f(v) v^2 dv, \quad (5)$$

where θ_p is the angle between the polarization vector of the pump laser and the propagation vector of the probe laser. Of special interest is the magic angle $\theta_p = 54.74^\circ$. In this case $P_2(\cos \theta_p) = 0$, and the Doppler profile depends only on $f(v)$. Differentiating $D(w)$ with respect to w gives,²⁶

$$f(v) = -\frac{2}{v} \left. \frac{\partial D(w)}{\partial w} \right|_{|w|=v}. \quad (6)$$

This method works for all values of β but requires a high signal to noise ratio to recover $f(v)$ accurately.

B. VADS

With this technique a delay is introduced between the pump and probe laser pulses. It is required that the lasers are aligned coaxially ($\theta_p = \pi/2$). At sufficiently long delay a particle with a velocity component perpendicular to the propagation direction of the probe beam will fly out of the detection region. This discrimination effect greatly enhances the velocity resolution of the experiment.

The VADS spectrum can be derived from the conventional Doppler profile by subtracting out the undetected particles. The fraction of particles detected after a delay t is given by a delay function, $F(v, w, t)$. If both laser beams have Gaussian profiles, the delay function is given by³⁰

$$F(v, w, t) = \frac{\rho^2}{\rho^2 + \alpha^2 t^2} e^{-[(v^2 - w^2)t^2/\rho^2 + \alpha^2 t^2]}, \quad (7)$$

where $\rho^2 = r_1^2 + r_2^2$, r_1 and r_2 are the Gaussian widths of the pump and probe laser profiles, and α is the most probable thermal speed of the parent molecule normal to the optical axis. With this correction factor the VADS profile is given by

$$D(w, t) = \int_{|w|}^{\infty} \frac{1}{2v} \left[1 - \frac{1}{2} \beta P_2(w/v) \right] \times F(v, w, t) f(v) v^2 dv. \quad (8)$$

If β is zero, the product speed distribution $f(v)$ can be extracted from a VADS profile by differentiating $D(w, t)$ with respect to w ; i.e.,

$$f(v) = -\frac{2}{w} \frac{\rho^2 + \alpha^2 t^2}{\rho^2} \left. \frac{dD(w, t)}{dw} \right|_{|w|=v} + \frac{4t^2}{\rho^2} \left. D(w, t) \right|_{|w|=v}. \quad (9)$$

While in principle ρ and α could be measured, in practice they are treated as free parameters that were adjusted to yield the same $f(v)$ for different values of t .

C. Deconvolution

It is necessary to correct the observed profiles for the nonzero bandwidth of the probe laser and thermal motion of the parent molecules along the line-of-sight. This is especially important for heavy fragments such as Cl and HCl. The deconvolution procedure has been discussed elsewhere.^{31–33} Briefly, $D(w, t)$ is expanded in a set of even harmonic oscillator functions, i.e.,

$$D(w, t) = \sum_{j=0}^{n-1} a_j \phi_{2j}(w, \lambda), \quad (10)$$

where $\Phi_{2i}(w, \lambda)$ is the $(2i)$ th harmonic oscillator eigenfunction with width parameter λ . The expansion coefficients a_i are given by the integral of the product of $\Phi_{2i}(w, \lambda)$ and the experimental Doppler profile. Both forward and inverse convolution of Φ_{2i} with a Gaussian transfer function can be performed analytically,³³ where the transfer function is a convolution of the one dimensional Maxwell–Boltzmann speed distribution and a Gaussian étalon transmission function. For our data, we found that 10 basis functions were sufficient to obtain a satisfactory fit of $D(w, t)$. The parameter λ was optimized by minimizing χ^2 . The fitted function was then deconvoluted term by term, and $f(v)$ was obtained by analytical differentiation.

IV. RESULTS

A. HCl fragments

The angular distribution of the HCl fragments was measured by Umemoto *et al.*¹⁴ using a TOF-MS and rotating the polarization direction of the photolysis laser. Their work showed a nearly isotropic distribution ($\beta = 0.088 \pm 0.015$) for HCl averaged over all rovibrational states. Since one of our present objectives is to understand the reason for the difference between the rotational state distributions for HCl($v'' = 0$) and HCl($v'' > 0$), it is necessary to determine whether β depends on v'' and J'' . To do so, we measured conventional (zero delay) Doppler profiles of the HCl(v'', J'') fragments with the polarization vector of the pump laser both parallel and perpendicular to the propagation direction of the probe laser. The parallel and perpendicular profiles, D_{\parallel} and D_{\perp} , were recorded for the $R(1)$, $P(13)$, and $Q(11)$ lines of the $0 \leftarrow 0$ band, the $R(1)$ and $P(9)$ lines of the $1 \leftarrow 1$ band, and the $R(3)$ line of the $1 \leftarrow 2$ band of the $F \leftarrow X$ transition. An example is shown in Fig. 2 for HCl($v'' = 0, J'' = 11$). In every case D_{\parallel} and D_{\perp} were indistinguishable, indicating that β is close to zero. In addition, conventional Doppler profiles for the $Q(11)$ and $P(13)$ and delayed Doppler profiles for the $Q(11)$ and $R(11)$ lines of the $0 \leftarrow 0$ band were nearly identical, indicating that $\mathbf{v} \cdot \mathbf{J}$ correlation is negligible.

Since HCl recoils isotropically, it is possible to use VADS to measure the speed distribution function. We accordingly measured the VADS profiles for a number of rovibrational lines using both short ($t = 600$ ns) and long ($t = 1400$ ns) delay times under otherwise identical conditions. The following profiles were recorded: $R(1)$, $R(4)$, $R(8-12)$, $P(3-5)$, $P(13)$, and $Q(11-14)$ lines of the $0 \leftarrow 0$ band, $R(5)$ and $R(12)$ of the $0 \leftarrow 1$ band, $R(1)$, $R(7)$, $P(8)$, and $P(9)$ of

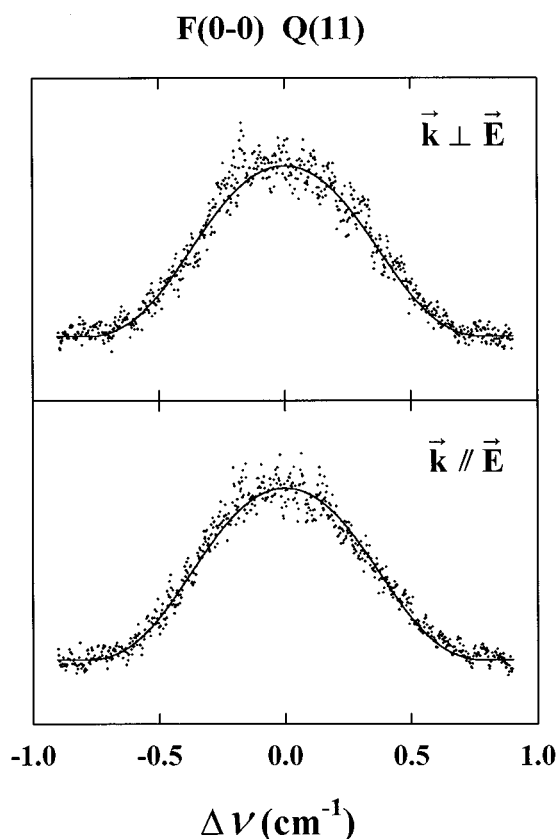


FIG. 2. Doppler profiles for the $Q(11)$ line of the $F^1\Delta, v''=0 \leftarrow X^1\Sigma^+, v''=0$ transition of HCl. Upper panel is for the propagation vector of the probe laser perpendicular to the polarization vector of the photolysis laser; lower panel is for the vectors parallel to each other. The curve in the upper panel is a least squares fit of a linear combination of harmonic oscillator functions. The curve in the lower panel is a duplicate of the upper panel curve.

the $1 \leftarrow 1$ band, and $R(3)$ and $P(10)$ of the $1 \leftarrow 2$ band. Typical examples are plotted in Figs. 3 and 4 for both short and long

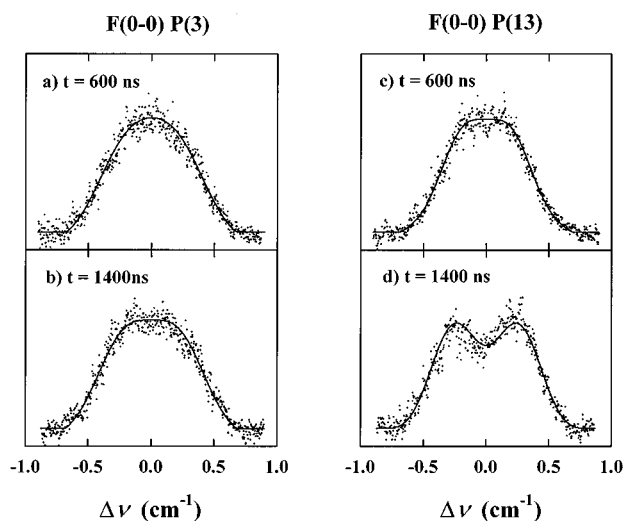


FIG. 3. Velocity-aligned Doppler spectra (VADS) for HCl($v''=0$), with short and long delays. (a) and (b) are for low rotation ($J''=3$), while (c) and (d) are for high rotation ($J''=13$). Curves are least squares fits, as described in the text.

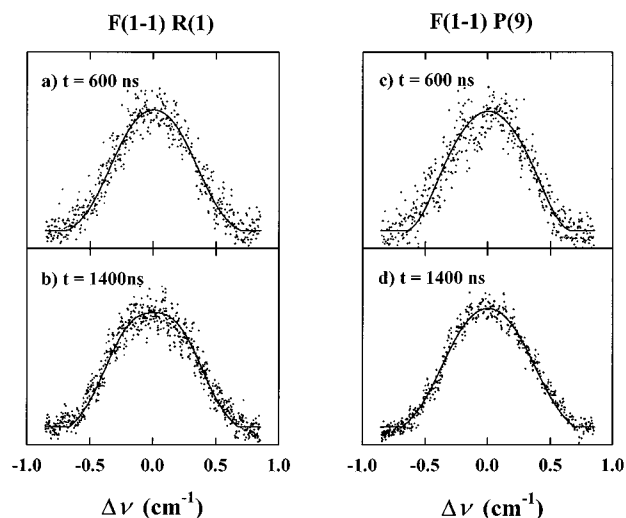


FIG. 4. Same as Fig. 3, only for HCl ($v''=1$). VADS profile are for $J''=1$ [(a) and (b)] and $J''=9$ [(c) and (d)].

delays. Figure 3 shows the VADS profiles for the $P(3)$ and $P(13)$ lines of the $0 \leftarrow 0$ band, while Fig. 4 shows $R(1)$ and $P(9)$ of the $1 \leftarrow 1$ band. These examples display a qualitative difference between the profiles for low and high J'' and for $v''=0$ and $v''=1$. For $v''=0$, $J''=3$, increasing the delay broadened the profile somewhat but did not introduce any additional structure, while for $v''=0$, $J''=13$ the profile splits into two peaks at long delay. For $v''=1$, on the other hand, both low and high J'' show a single maximum at long delay.

The speed distribution functions were extracted from the VADS profiles, using the procedure described in the previous section. Values of $\rho \approx 1.0$ mm and $\alpha \approx 150$ K were obtained by simultaneously minimizing χ^2 for $t=600$ and 1400 ns. The ρ value is in good agreement with an experimental estimate. The distribution functions recovered from all the VADS profiles are shown in Fig. 5. It should be noted that $f(v)$ plotted without the v^2 volume factor is a one-dimensional distribution function. The uniqueness of the high J'' , $v''=0$ distributions is apparent; the splitting of the VADS profiles at long t is clearly caused by a distribution function peaked at $v > 0$, so that at long delay the recoiling fragments split into two populations, one moving towards and the other away from the detector. The 1D average speed, $\langle v \rangle = \int v f(v) dv$, plotted in Fig. 6, shows a monotonic increase with J'' for $v''=0$. There is no apparent trend for $v'' > 0$.

To check the self-consistency of using the VADS method, we calculated from $f(v)$ an upper bound on β . From Eq. (5) the difference between D_{\parallel} and D_{\perp} is given by

$$\Delta D(w) = \frac{3}{2} \beta \int_{|w|}^{\infty} [P_2(w/v)] f(v) v dv. \quad (11)$$

Comparing this function with the experimental values of $D_{\parallel} - D_{\perp}$ gives $|\beta| < 0.1$, in agreement with Umemoto *et al.*¹⁴

The 3D translational energy distributions, $p(E_t)$, show little variation with J'' even for $v''=0$. The reason for this is that the v^2 weighing factor obscures the systematic trends visible in the 1D projections. The 3D distributions for all

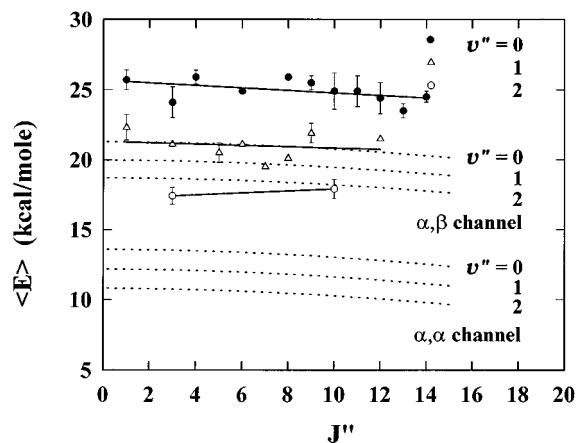


FIG. 8. Average kinetic energy of $\text{HCl}(v'', J)$ as a function of rotational quantum number for $v''=0$ (solid circles), 1 (triangles), and 2 (open circles). Solid lines are linear least squares fits. Dashed lines are the prior values for three-center (upper set) and four-center (lower set) elimination.

evident for all four compounds. The two peaks are of comparable height for VCl, while for the DCE isomers the low energy peak is much higher. For the $\text{Cl}(^2P_{1/2})$ product, $p(E_t)$ is shifted towards higher energy in each case. For VCl there is only a small shoulder at low energy; for *trans*-DCE the two peaks appear to have merged, while for *cis*- and 1,1-DCE and VCl the peaks are of comparable height. Similar trends are also apparent in Table I, where the mean and maximum energies are listed. The mean kinetic energy of $\text{Cl}(^2P_{1/2})$ is on the average 6 kcal/mol greater than for $\text{Cl}(^2P_{3/2})$. The maximum energies differ by a comparable amount.

V. DISCUSSION

A. HCl molecular elimination

The ground state electronic configuration of vinyl chloride is $(1a')^2(2a')^2(3a')^2(4a')^2(5a')^2(6a')^2(1a'')^2(7a')^2(2a'')^2$. Absorption of a 193 nm photon induces a $\pi \rightarrow \pi^*$ transition to the $1^1A'$ state with configuration $\dots(7a')^2(2a'')^1(3a'')^1$. Excited states lying below this energy are the $1^3A'$ ($\pi \rightarrow \pi^*$) and the $1^{1,3}A''$ ($\pi \rightarrow \sigma^*$) states, the latter having a $\dots(7a')^2(2a'')^1(8a')^1$ configuration. We mention for later reference a higher lying $n \rightarrow \sigma^*$ state with a $\dots(7a')^1(2a'')^2(8a')^1$ configuration. To determine on which PES the reaction may occur, we constructed correlation diagrams for HCl elimination along the different reaction paths shown in Figs. 10–12.³⁴ The vertical excitation energies for the low-lying electronic states of VCl, vinylidene, and acetylene were obtained from Ref. 35.

A number of conclusions may be drawn from these diagrams. (i) In all cases HCl elimination on the initially excited PES does not correlate with ground state products. (ii) In all cases HCl elimination on S_0 is allowed since the orbital occupation numbers in C_s symmetry are $(a')^{14}(a'')^4$ for reactants and products. This is in contrast to H_2 elimination from ethylene along a C_{2v} dissociation path, which is symmetry forbidden. A large barrier is nevertheless observed for VCl dissociation, showing that the C–Cl σ -bond does not completely destroy the C_{2v} symmetry. (iii) Triplet acetylene may

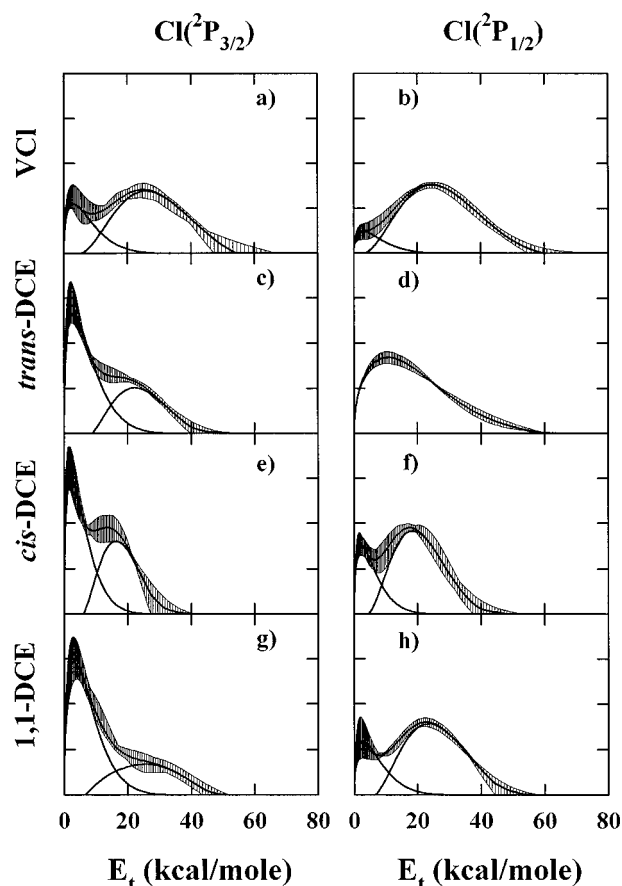


FIG. 9. Kinetic energy distributions for $\text{Cl}(^2P_{3/2})$ and $\text{Cl}(^2P_{1/2})$, obtained by inverting magic angle Doppler spectra. The shaded areas indicate the range observed for four scans. The heavy curves indicate the average profile and its decomposition into low and high energy components. The low energy components are prior distributions, while the high energy components were obtained by subtraction.

be formed in both linear (Fig. 11) and *cis*-states (Fig. 12), while dissociation to form triplet vinylidene (Fig. 10) is symmetry forbidden. Since $\text{VCl}(^3A'')$ and $\text{H}_2\text{C}=\text{C}:(^3B_2) + \text{HCl}(X^1\Sigma^+)$ have the same overall state symmetry (A'') but different occupation numbers (15,3 vs 13,5), a large barrier must exist for this path.

Triplet vinylidene was reported by Fahr and Laufer³⁶ as a major product at 137, 139, and 151 nm. They inferred that the most probable pathway involves crossing of the initially excited singlet to a long-lived triplet state. In the present

TABLE I. Maximum and average kinetic energies of the Cl fragment.^a

Molecule	Fragment energy (kcal/mol)			
	$\text{Cl}(^2P_{3/2})$		$\text{Cl}(^2P_{1/2})$	
	E_{max}^a	$\langle E \rangle^b$	E_{max}	$\langle E \rangle$
VCl	45–65	23	55–70	25
<i>trans</i> -DCE	40–55	14	55–60	19
<i>cis</i> -DCE	25–40	12	35–50	17
1,1-DCE	45–50	12	45–60	22

^aThe range is the spread in maximum energies indicated by the shaded regions in Fig. 9.

^bMean energy for the average distribution.

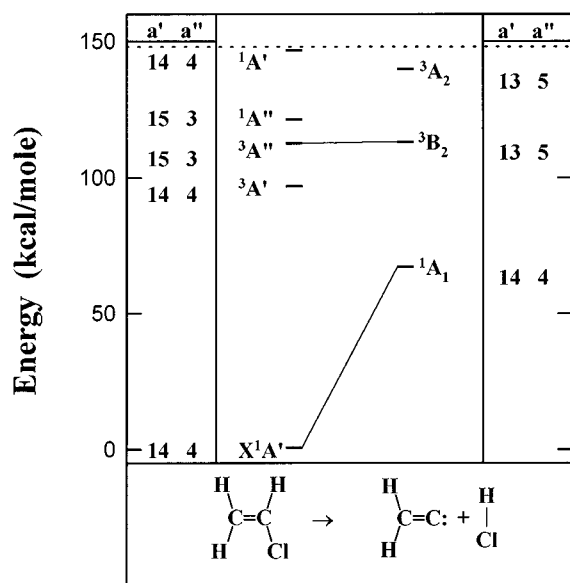


FIG. 10. State correlation diagram for the decomposition of VCl to produce HCl+vinylidene. The numbers in the left and right columns indicate the occupation numbers for a' and a'' orbitals having C_s symmetry, with σ_{xz} as the molecular plane. State labels in the center of the diagram refer to VCl on the left and vinylidene on the right. The photon energy is indicated by the horizontal dashed line.

experiment, where there is much less available energy, the production of a triplet fragment is unlikely. Production of 3B_1 acetylene would leave a maximum of 42 kcal/mol available for translation and HCl internal energy, whereas we observed up to 74 kcal/mol for these degrees of freedom³⁷ (see Fig. 7), with no indication of a bimodal kinetic energy distribution. Moreover, the triplet state of the parent molecule was not

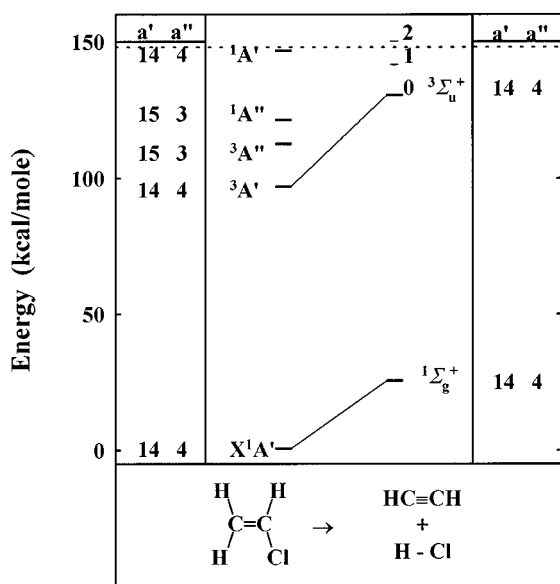


FIG. 11. State correlation diagram for the decomposition of VCl to produce HCl+ linear acetylene. Notation is the same as in Fig. 10, except that the product symbols refer to the electronic states of acetylene and vibrational quantum numbers of HCl.

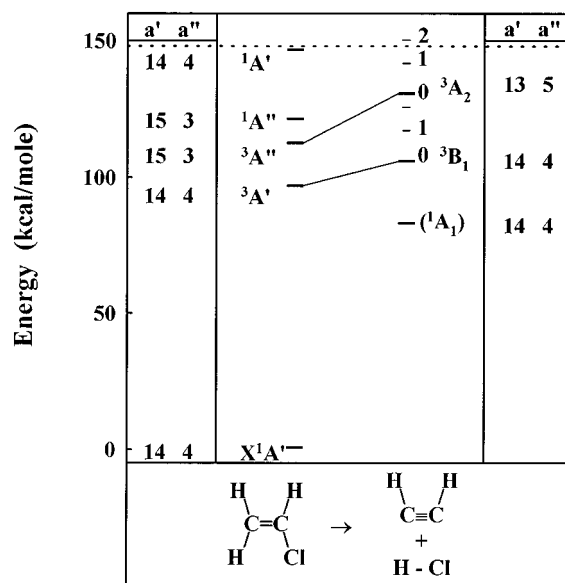


FIG. 12. State correlation diagram for the decomposition of VCl to produce HCl+ *cis*-bent acetylene. Notation is the same as in Fig. 10, except that the product symbols refer to the electronic states of acetylene and vibrational quantum numbers of HCl. The 1A_1 state of *cis*-HCCH is unstable.

detected in the electron diffraction measurement of Ewbank *et al.*³⁸ at 193 nm. It follows that the most likely mechanism is internal conversion followed by HCl elimination on the ground PES. In the case of ethylene, internal conversion is a highly efficient process, resulting from pseudomigration of a H atom to form a zwitterionic state, which interacts very strongly with the ground state.³⁹ A similar mechanism is expected for VCl.

Riehl and Morokuma²¹ located three transition states for HCl elimination on the ground PES, corresponding to α,α and α,β elimination and a four-center "knockout" mechanism following H migration. The H-Cl bond lengths in these transition states are, respectively, 1.436, 1.789, and 2.356 Å, as compared with 1.269 Å for free HCl and 2.374 Å for HCl in the parent molecule. The exit barriers heights (measured with respect to the separated products) are 2.5, 52.6, and 62.8 kcal/mol. Of these, the α,α transition state is closest to the product geometry, with only a small exit barrier.

Since the reaction occurs on the ground PES, it is likely to live for many vibrational periods. If the molecule eventually reacts along the α,α path, which has a "loose" transition state and small exit barrier, we would expect the fragments to have a statistical state distribution.² To test this possibility we compared the observed $p(E_t)$ with the expectation from a prior, statistical model. This model assumes that all accessible quantum states are equally populated, so that all the available energy is partitioned evenly among all degrees of freedom. The prior kinetic energy distribution function is⁴⁰

$$p^0(v, j, E_t | E_{av1}) \propto E_t^{1/2} \int_0^{E_{av1} - E_t} \rho_v(E_v) \times (E_{av1} - E_t - E_v)^{1/2} dE_v, \quad (12)$$

where $\rho_v(E_v)$ is the continuous density of vibrational states,

calculated using the Whitten–Rabinovitch approximation,⁴¹ and E_{avl} is the available energy.¹⁸ For the four-center process $E_{\text{avl}} = 124.2 \pm 0.4$ kcal/mol, while for three-center elimination $E_{\text{avl}} = 81 \pm 2$ kcal/mol. The prior distributions $p^0(E_t)$ are shown in Fig. 7, and the prior values of the average energy $\langle E_t \rangle^0$ are given in Fig. 8. It is apparent from these figures that the three-center prior distributions do not match the data, while the four-center prior distributions are in much better agreement, with the agreement improving as v'' increases from 0 to 2.

While there is no requirement for a four-center mechanism to produce a statistical distribution, it is difficult to reconcile a non-statistical distribution with a three-center path. Our result is in seeming contradiction with our earlier finding that the HCl yield from *d*-VCl is 25% of that from normal VCl, showing a preference for α, α elimination. This problem is related to the rotational scrambling process discussed in the Introduction, since any mechanism which accounts for the isotopic yields must also explain why the rotational distributions of HCl produced from VCl and *d*-VCl are identical.

From the isotope experiment we deduce that HCl is eliminated primarily by an α, α mechanism. We also know that the vinylidene fragment isomerizes rapidly to form acetylene. A key question is the relative time scales of the elimination and isomerization steps. At one limit the processes are stepwise, in which case none of the isomerization energy is available to HCl. At the other limit, the steps are concerted and synchronous, which means that HCl flies off at the same instant that the vinylidene H atom migrates from one carbon atom to the other. In this case we would expect a highly nonstatistical translational energy distribution.⁴² The mechanism that we propose lies between these two limits, namely, a concerted but nonsynchronous pair of steps. The elimination reaction begins by passage through the three-center transition state (A2 in Fig. 1). At this point the fragments are still moving fairly slowly. The most probable speed in the three-center statistical distribution is 0.024 Å/fs, while the lifetime for isomerization of vinylidene has been estimated to lie between 40 and 200 fs, with a lower bound of 27 fs.²⁴ As the fragments separate a hydrogen atom on vinylidene migrates to form acetylene (passing through A21 in Fig. 1), releasing an additional 53 kcal/mol, some of which is converted to relative translational energy. This additional energy release is not along the reaction coordinate, and much of it goes into acetylene vibration.

To explain the identical rotational state distributions for HCl produced from VCl and *d*-VCl, we propose that isotopic scrambling occurs in a separate step *before* the molecule reaches transition state A2. Riehl and Morokuma²¹ found that the lowest energy transition state (C1 in Fig. 1) is reached by H atom migration to produce the stable $\text{CH}_3\text{=CCl}$ radical. Formation of this species and the return to VCl competes with three-center elimination. Since internal conversion from the π, π^* surface is initiated by migration of a H atom,³⁹ the conformation of the molecule on the ground PES already favors this low energy path. In the case of *d*-VCl we propose that isotopic scrambling occurs by D migration to form $\text{CH}_2\text{D=CCl}$, followed by H back-migration

to give CHD=CHCl . The 25% relative yield of HCl from *d*-VCl indicates that elimination of DCl through transition state A2 is more probable than isotopic scrambling through the radical intermediate.

To explain the dichotomy between the rotational state distributions for $\text{HCl}(v''=0)$ and $\text{HCl}(v''>0)$, we propose that the reaction is vibrationally adiabatic. Since the vibrational frequency of HCl is lower in the transition state than in the isolated molecule, the vibrationally adiabatic barrier height should decrease with vibrational quantum number. This idea is consistent with the observation in Fig. 8 that $\langle E_t \rangle$ decreases by approximately one-half of the HCl vibrational spacing per unit increase in v'' . Since the exit barrier for α, α elimination is much smaller than the vibrational spacing of free HCl, it is plausible that the adiabatic barrier disappears entirely for $v''>0$.

To restate this last point, as the fragments separate they are repelled by two barriers, a small, vibrationally adiabatic barrier which is greatest for $\text{HCl}(v''=0)$, and a large exit barrier caused by vinylidene–acetylene isomerization. These barriers have qualitatively different effects. Repulsion by the former is directed along the reaction coordinate. We speculate that the hotter rotational population of $\text{HCl}(v''=0)$ and the 1D scalar E_t – J correlation shown in Fig. 6, are caused by this direct energy release. A similar correlation between rotation and translation was observed by Jiminez *et al.*⁴³ in the photodissociation of 3-cyclopentenone. Passage over the second barrier releases energy, which is partitioned between intramolecular excitation of acetylene and intermolecular repulsion of the separating fragments. Since the reaction is nonsynchronous we cannot predict how much the energy distribution will deviate from the statistical limit. It would be highly desirable to perform dynamical calculations on a globally accurate PES to see whether our proposed mechanism can account for the observed rotational and translational energy distributions.

Based on our model, we expect that slowing down the vinylidene–acetylene isomerization step should have a dramatic effect on the dynamics of HCl elimination. In a study of the infrared multiphoton excitation of 2-chloro-1,1-difluoroethylene ($\text{F}_2\text{C=CHCl, CFE}$), Reiser *et al.*⁴⁴ found that $\text{F}_2\text{C=C:}$ is a long-lived species with essentially no rearrangement taking place to form perfluoro-acetylene. A semiquantitative MO calculation⁴⁵ gives an activation barrier for the rearrangement $\text{F}_2\text{C=C:} \rightarrow \text{FC}\equiv\text{CF}$ of ~ 60 kcal/mol, as compared with ~ 3.0 kcal/mol for the rearrangement of vinylidene to acetylene.⁴⁶ Using IR multiphoton excitation of CFE with TOF analysis, Sudbø *et al.*⁴⁷ found that $p(E_t)$ could be fit with a RRKM model with $\langle E_t \rangle \approx 1.0$ kcal/mol, and that essentially no translational energy is released to the fragments after they pass the critical configuration in the exit channel. In our own preliminary study of the UV excitation of CFE, we observed a Boltzmann-type rotational state distribution for $\text{HCl}(v''=0)$.⁴⁸ These results are consistent with our understanding of the VCl reaction. In this case isomerization of the perfluoro-vinylidene radical takes place too slowly to release energy to the fragments, and the product state distributions are statistical.

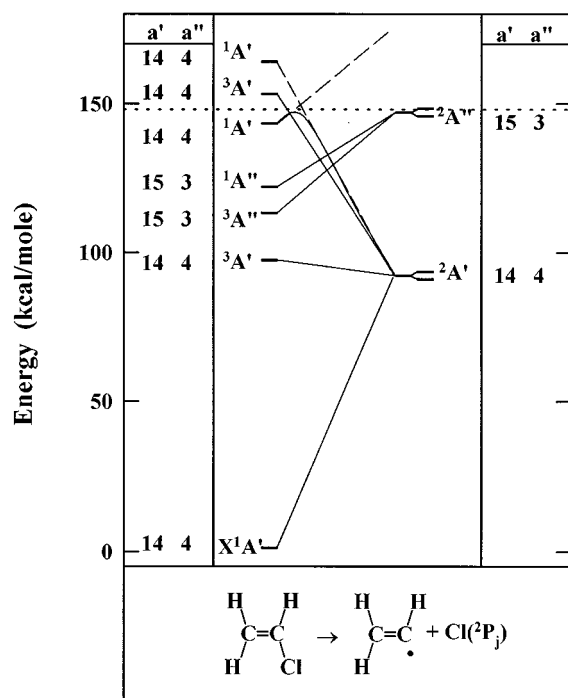


FIG. 13. State correlation diagram for the decomposition of VCl to produce a vinyl radical and a Cl atom. Notation is the same as in Fig. 9, except that the product symbols refer to the electronic states of the vinyl radical. Also, the spin-orbit splitting of Cl is indicated.

B. Cl atomic detachment

Figure 13 shows the correlation diagram for Cl detachment from VCl with C_s symmetry. The ground state fragments have a $(7a')^1(2a'')^2(8a')^1$ configuration, which is the same as that of the $^1A'(n,\sigma^*)$ state of VCl. Because of an avoided crossing of the n,σ^* and π,π^* surfaces (shown as dashed lines in Fig. 13), the products correlate adiabatically with the π,π^* state. Although the ground (π^2) state of VCl and the ground state fragments have different orbital configurations, they are nevertheless correlated because of configuration interaction of the $^1A'$ species of VCl. On the other hand, the $^1A''(\pi,\sigma^*)$ state of VCl correlates with the first

electronically excited state of the vinyl radical and does not mix with the ground state. We cannot rule this out as a conceivable reaction path, however, since it is possible that in nonplanar geometry the π,π^* and π,σ^* states are mixed. From these considerations we see that there are two distinct paths for Cl detachment, direct reaction on the n,σ^* surface, and indirect reaction on the ground PES following internal conversion.

Our data in Fig. 9 show two components in the translational energy distributions of $\text{Cl}(^2P_{3/2})$ and $\text{Cl}(^2P_{1/2})$ produced by photodissociation of VCl and the DCE isomers. Similar results were obtained by other workers. Umemoto *et al.*¹⁴ observed bimodal distributions in the TOF spectra of the Cl atoms. Bimodal distributions of the individual spin-orbit states were observed by Mo *et al.*¹⁸ using polarized Doppler spectroscopy and by Suzuki *et al.*²⁰ using photofragment imaging. Our data are in good qualitative agreement with the data of Umemoto *et al.*¹⁴ and Suzuki *et al.*,²⁰ except that the latter observed a more pronounced high energy shoulder in $\text{Cl}(^2P_{1/2})$ produced from *trans*-DCE.

A natural interpretation of our data is that the bimodal distributions are produced by the two reaction paths described above, with the low energy component coming from reaction on the ground PES and the high energy component corresponding to reaction on the excited surface, as first suggested by Umemoto *et al.*¹⁴ Here too we expect the reaction on the ground surface to be statistical. A comparison of $p(E_t)$ with the prior distributions (normalized by an adjustable scaling factor) in Fig. 9 confirms that this is the case. The kinetic energy distributions for the high energy component were determined by subtracting the priors from the total distributions. The average energies of the high energy component listed in Table II and the maximum energies listed in Table I increase in the order of *cis*-, *trans*-, 1,1-, and VCl. This sequence may reflect the relative locations of the non-adiabatic crossing of the excited surfaces. For an outer-limb crossing the recoil energy should increase with crossing distance, while the reverse is expected for an inner-limb crossing.⁴⁹

After this paper was completed we learned of a new study by Ebata *et al.*⁵⁰ in which the sum of the quantum

TABLE II. Properties of Cl produced on the ground and excited potential energy surfaces.

Molecule	Γ_{tot}^c	$P_f(^2P_{3/2})^d$	$P_f(^2P_{1/2})^e$	Ground PES ^a			Excited PES ^b		
				Γ_0	E_{av}	E_{mp}	Γ_1	E_{av}	E_{mp}
VCl	0.30	0.76	0.89	0.14	1.6	3.0	0.35	22	25
<i>trans</i> -DCE	0.15	0.42	f	f	4.3 ^g	2.9 ^g	f	10 ^g	23 ^g
<i>cis</i> -DCE	0.17	0.47	0.72	0.09	3.0	2.6	0.26	9.6	16
1,1-DCE	0.28	0.35	0.76	0.10	4.1	2.8	0.60	12	25

^aProperties of the Cl atoms produced on the ground PES, summed over both spin-orbit states. The most probable and mean kinetic energies are expressed in kcal/mol and are sums over both spin-orbit states.

^bProperties of the Cl atoms produced on the excited PES, summed over both spin-orbit states.

^cTotal branching ratio, taken from Ref. 18.

^dFraction of $\text{Cl}(^2P_{3/2})$ produced on the excited PES, e.g., for VCl, 76% of $\text{Cl}(^2P_{3/2})$ is produced on the excited PES and 24% on the ground PES.

^eFraction of $\text{Cl}(^2P_{1/2})$ produced on the excited PES.

^fThe speed energy distribution for $\text{Cl}(^2P_{1/2})$ produced from *trans*-DCE could not be resolved into slow and fast components.

^gCalculated for $\text{Cl}(^2P_{3/2})$ only.

yields for Cl and HCl produced from *trans*-DCE at 193 nm was found to be greater than unity. Their data implies that some of the parent molecules decompose to yield two Cl atoms. A kinematic analysis shows that when this occurs the kinetic energy distributions of both atoms lie under the statistical component of $p(E_i)$ (Fig. 9). This result is consistent with our assignment of the high energy component of $p(E_i)$ to reaction on an excited PES and the low energy component to reaction on the ground PES.

A striking property of the distribution functions shown in Fig. 9 and Tables I and II is the tendency for $\text{Cl}(^2P_{1/2})$ to have more kinetic energy than $\text{Cl}(^2P_{3/2})$. One possible explanation is that dissociation on S_0 gives mainly $\text{Cl}(^2P_{3/2})$ while dissociation on the (n,σ^*) surface gives a mixture of both spin-orbit states. To test this idea we calculated the spin-orbit branching ratio for each surface, as follows. The overall branching ratio,

$$\Gamma_{\text{tot}} = [\text{Cl}(^2P_{1/2})]/[\text{Cl}(^2P_{3/2})], \quad (13)$$

was measured by Mo *et al.*¹⁸ Next we label the areas under each component of $p(E_i)$ as $F(3/2,s)$, $F(3/2,f)$, $F(1/2,s)$, $F(1/2,f)$, where s and f refer to the low and high energy components, and $F(j,s) + F(j,f) = 1$ for each spin-orbit state. The branching ratios for the individual surfaces are then given by

$$\Gamma_0 = [F(1/2,s)/F(3/2,s)]\Gamma_{\text{tot}} \quad (14)$$

for the ground PES, and by

$$\Gamma_1 = [F(1/2,f)/F(3/2,f)]\Gamma_{\text{tot}} \quad (15)$$

for the (n,σ^*) surface. The results listed in Table II show that reaction on the ground surfaces gives >85% $\text{Cl}(^2P_{3/2})$, while on the excited surface 21%–59% of the Cl atoms are in the $j=1/2$ state.

One possible explanation of these branching ratios is adiabatic correlation between the parent molecule and the radical fragments. The ground PES necessarily correlates with $\text{Cl}(^2P_{3/2})$. A very crude model in which the vinyl radical is described as a $^2S_{1/2}$ atom predicts that $^1(n,\sigma^*)$ also correlates with $\text{Cl}(^2P_{3/2})$.⁵¹ A more sophisticated treatment, including spin-orbit coupling of the excited states, is likely to correlate the excited state of the parent molecule with both spin-orbit states of Cl. A criterion for adiabatic dissociation is that the Massey adiabaticity parameter,

$$\xi = R\Delta E_{\text{so}}/\hbar v, \quad (16)$$

be greater than unity.⁵² In Eq. (16), R is a characteristic recoil distance, $\Delta E_{\text{so}} = 881 \text{ cm}^{-1}$ is the fine structure splitting of the Cl atom, and v is the recoil speed. Taking $R = 1 \text{ \AA}$, and setting v equal to the most probable speed ($1.8 \times 10^5 \text{ cm/s}$ on the ground PES and $3.9 \times 10^5 \text{ cm/s}$ on the excited PES), ξ has a value of 9.2 and 4.3 on the lower and upper surfaces, respectively. These large values are consistent with an adiabatic mechanism, as compared with $\xi = 0.8$ for the photodissociation of HCl at 193 nm, assuming the same value for R .

Another factor contributing to Γ is scrambling of the spin-orbit populations in the asymptotic region.⁵¹ In the high energy limit, a statistical value of $\Gamma = 1/2$ is predicted. The faster Cl atoms produced on the n,σ^* surface should have a

greater probability of undergoing a nonadiabatic transition to the $j=1/2$ state.⁵³ This point is consistent with our observation that Cl produced from *cis*-DCE has both the lowest kinetic energy and the lowest value of Γ_1 .

While we cannot determine the relative importance of structural vs dynamic factors, both of the proposed effects predict $\Gamma_1 > \Gamma_0$, as observed. One must, nevertheless, be cautious in invoking such simple models to explain the fine structure population of the fragments, especially when surface crossing is involved. Recent work in this laboratory on the predissociation of Rydberg states of HCl has shown that Γ is very sensitive to the potential energy surface,⁵⁴ and considerations such as adiabatic vs sudden recoil are insufficient in the case of HCl for predicting the asymptotic populations.

VI. SUMMARY AND CONCLUSIONS

We have used velocity aligned Doppler spectroscopy to measure the kinetic energy distribution functions of different rovibrational states of HCl produced in the 193 nm photodissociation of vinyl chloride. The average kinetic energy was found to vary inversely with the vibrational energy of HCl. For $\text{HCl}(v''=0)$ the one-dimensional kinetic energy was found to increase with rotational energy, while for $v'' > 0$ there was no apparent rotational dependence. A statistical model assuming three-center elimination is inconsistent with the data, while a four-center mechanism on the ground potential energy surface is in better agreement. This result is in seeming contradiction with an earlier isotopic experiment which showed that HCl elimination is primarily α,α . To reconcile all of our observations we propose a mechanism in which three-center HCl elimination followed by vinylidene-acetylene isomerization occurs in a concerted, nonsynchronous fashion. It is further proposed that isotopic scrambling in vinyl chloride occurs by hydrogen atom migration, producing the stable $\text{CH}_3=\text{CCl}\cdot$ intermediate. The dichotomy between the rotational state populations for $\text{HCl}(v''=0)$ and $\text{HCl}(v'' > 0)$ is explained by a vibrationally adiabatic mechanism.

Magic angle Doppler spectroscopy was used to measure the kinetic energy distribution functions of $\text{Cl}(^2P_{3/2})$ and $\text{Cl}(^2P_{1/2})$ produced in the 193 nm photodissociation of vinyl chloride and the three dichloroethylene isomers. Bimodal energy distributions were observed for both spin-orbit states, indicating competitive reactions on two potential energy surfaces. The $\text{Cl}(^2P_{1/2})$ product was found to have consistently more kinetic energy than $\text{Cl}(^2P_{3/2})$. Adiabatic correlation, with some scrambling in the asymptotic region, is proposed to explain the spin-orbit branching ratios.

ACKNOWLEDGMENTS

We wish to thank Professor Keiji Morokuma for many helpful discussions and for providing us with copies of Refs. 21 and 22 prior to their publication. We also wish to thank Professors Stephen Leone and Joseph Cline for helpful discussions regarding the VADS technique. This work was supported by the National Science Foundation (Grant Nos.

